# EXPERIMENTAL INVESTIGATION OF MECHANICAL FASTENERS REGARDING THEIR INFLUENCE ON CRACK GROWTH IN ADHESIVELY BONDED CRFP-JOINTS SUBJECTED TO FATIGUE LOADING

R. Sachse[1], A.K. Pickett[1], W. Adebahr[2], M. Klein[1], M. Käß[1], P. Middendorf[1]

[1]Institute of Aircraft Design, University of Stuttgart
Pfaffenwaldring 31, 70569 Stuttgart
Email: sachse@ifb.uni-stuttgart.de, web page: http://www.ifb.uni-stuttgart.de

[2]Institut für Kunstofftechnik, University of Stuttgart
Pfaffenwaldring 31, 70569 Stuttgart
Email: wolfgang.adebahr@ikt.uni-stuttgart.de, web page: http://www.ikt.uni-stuttgart.de/

**Keywords:** Adhesive Bonding, Crack Arresting Mechanism, Fatigue Delamination, Hybrid Joints

## ABSTRACT

A screening test program has been performed for different hybrid joint configuration investigating the effect of mechanical fasteners on the crack growth in adhesively bonded CFRP joints subjected to fatigue loading. The rivetless nut plate joint was selected as the baseline for this investigation. In order to separately investigate the effect of local reinforcement, additional pin configurations were studied considering different interfaces between the pin and the hole.

The test results suggest that the fasteners have no influence on an approaching crack. However, once the crack passes the fastener, it is being slowed down. The rate of crack speed reduction strongly depends on the type of fastener. In case of the rivetless nut plate joint the crack was virtually arrested 10mm behind the fastener.

## 1 INTRODUCTION

In recent years the application of carbon fiber reinforced plastics (CFRP) has gained increasing attention in the aerospace and automotive industries. Effective joining of these CFRP parts is a central question during the design process. While metal parts in aircraft structures are primarily riveted or bolted, this approach must be questioned for CFRP joints. Mechanical fasteners usually require drilling of the joining members, which in the case of CFRP is accompanied by significant wearout of the drill, the formation of dust, as well as probable delamination damage inside the composite. Adhesive bonding can be considered a promising alternative for thin-walled CFRP structures. It avoids the undesirable cutting of continuous fibers from drilling and allows a distributed transfer of stresses between the two sheets to be joined.

Despite the many technical advantages of adhesive bonding over mechanical fastening, aerospace certification regulations and corresponding means of compliance do not allow the use of purely adhesively bonded primary CFRP structures. Instead, a combination of riveting and bonding (or shimming) must be used in which the mechanical fasteners must be able to carry limit load once the adhesive bondline has completely failed. Among other specifications, these main means of compliance are documented in AC20-107B and result from in-service premature failure of the adhesive bondline. [1] [2]

It is the aim of the EU funded FP7 project BOPACS [2] to investigate the application of alternative features, or so-called ‘crack arresting’ mechanisms, that help arrest the failure of a debonding adhesive joint. While initial cracks can occur locally due to weak bonds or impact damage, these features shall arrest the crack in a way that the capability to withstand the required loads is still given.

It has been shown by many researchers that fatigue loading is critical to the integrity of adhesive joints. Crack propagation in previously damaged bondlines can occur already at a small percentage of the static strength [3] [4] [5] [6] [7]. A dominant factor influencing the rate at which a crack propagates under fatigue loading is the mixed-mode ratio. Pure mode I and II ratios have been respectively investigated using the double cantilever beam (DCB) specimen for peeling mode and the end-notched flexure (ENF) or end loaded split (ELS) specimens for shear mode loading. The results suggest that for thermoset based adhesive joints the crack growth rate in pure mode I loading can be several orders of magnitude faster than in pure mode II loading [6] [7].

Real aerospace structures are usually loaded in a combination of mode I and mode II loading. These realistic loading schemes can be represented using single lap joints (SLJ), cracked lap shear (CLS) specimens or a single leg bending (SLB) specimens [4] [5] [8] [9]. Due to its long overlap length, the CLS geometry represents the behaviour of bonded stringers particularly well, and consequently has been adopted here for fatigue studies [4].

Improved fatigue life of hybrid joints combining mechanical and adhesive bonding have been demonstrated [8] [10]. In particular it was found that low shear modulus adhesives allowed a more effective load distribution between the bondline and the fastener resulting in a retardation of damage initiation. Furthermore, recent studies [9] suggest that an interlaminar crack propagating within a composite can be arrested, or at least slowed down, in the vicinity of a fastener. As primary crack arresting mechanisms, the suppression of peeling mode stresses and the elastic influence on the structure were mentioned.

The present research is aimed at investigating different mechanical features regarding their effect on arresting cracks propagating in adhesively bonded CFRP joints. The focus lies on the identification of relevant crack arresting mechanisms, which shall enable an intelligent application of crack arresting features. Due to the local effect of these mechanical features it has been found essential to measure the crack front over the width of the test specimen.

## 2 TEST SPECIMEN DESIGN & CRACK ARRESTING FEATURES

The CLS specimen has been selected to investigate the influence of crack arresting features (CAF) on the crack propagation in adhesively bonded CFRP joints. The CLS specimen offers several advantages over other test geometries; most importantly it provides a realistic mixed mode ratio (MMR) which is almost constant over a large section of the coupon, giving a similarly constant strain energy release rate ($\Delta G$). For a force controlled constant amplitude fatigue loading, with a constant R-ratio and frequency, the latter results in a constant crack growth. The influence of a CAF can therefore be directly correlated to the rate at which the crack propagates.

Figure 1 gives a schematic representation of a CLS specimen. Its final design and the location of the CAF have been selected to meet the following requirements:

a) Aircraft relevant strain levels and composite stacking sequences
b) Sufficient distance to clamping area to avoid boundary effects
c) Sufficient space in front of the CAF to provide an initial undisturbed crack growth
d) Realistic testing time
e) Limitations due to the testing machine

The base laminate is made of Hexply IM7/8552 UD prepreg. A symmetric quasi-isotropic layup with a stacking sequence of $[0°, 45°, 90°, -45°, -45°, 90°, 45°, 0°]_s$ was used, resulting in a laminate thickness of approximately 2mm. The specimen width of 40mm was restricted by the clamping width of the testing machine. The unbonded section has a length of 75mm including an initial debonded length of 15mm. The initial debond was realized by inserting a Teflon foil prior to bonding. The two composite plates are bonded using the structural adhesive Scotch Weld 9323 B/A from 3M resulting in an effective bond length of 125mm. Additionally, a 40mm long clamping section is available. In order to avoid pre-bending and ensure axial loading of the specimen during clamping, a doubler was bonded to the free end of the single laminate. Finally tabs were bonded to the loaded ends to give a good load introduction to the specimens.

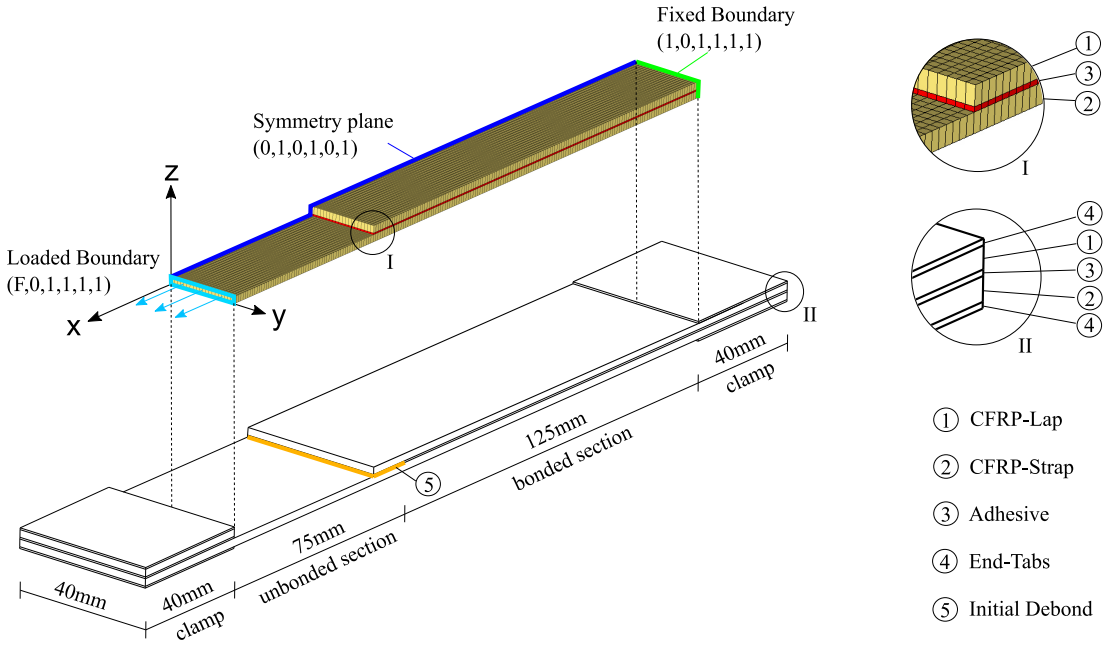


Figure 1: Schematic drawing and numerical model of the CLS specimen

In a preliminary study the crack growth rate for the given configuration was determined for several load levels with respect to the average strain in the unbonded laminate of the specimen. Within the project a strain level of $3000\mu strain$ was targeted. The corresponding crack growth rate, however, was so small that instead a maximum fatigue load ($F_{max}$) corresponding to approximately $4000\mu strain$ was chosen. The average crack growth rate for this load level was about 1mm per 1000 cycles.

## 2.1 NUMERICAL SIMULATIONS

Simple numerical simulations were performed to calculate $\Delta G$ and the MMR, and to determine the length of section where these parameters are approximately constant. $\Delta G$ and MMR are defined as follows:

$$\Delta G = G_{max} - G_{min} \tag{1}$$

$$MMR = \frac{G_{II} + G_{III}}{G_I + G_{II} + G_{III}} \tag{2}$$

With respect to Figure 1, $G_I$ refers to the peeling mode in the z-direction, and $G_{II}$ and $G_{III}$refer to shear modes in the x-z and y-z directions respectively.

The simulations were performed using Abaqus/Explicit. The laminate was modeled with standard shell elements assigning a linear elastic anisotropic material model. The adhesive was modeled using standard solid elements with a linear elastic isotropic material model. An offset was used so that the shell elements represent the adhesive interfaces. Material properties for the laminate and shear modulus of the adhesive were determined by in-house testing. The Young's modulus of the adhesive was calculated according Equation 3. All relevant material parameters are presented in Table 1 and Table 2.

$$E = 2G(1 + \nu) \tag{3}$$

| Engineering constant | | Value |
|---|---|---|
| $E_1$ | $[GPa]$ | 163 |
| $E_2$ | $[GPa]$ | 9.6 |
| $\upsilon_{12}$ | – | 0.31 |
| $G_{12}$ | $[GPa]$ | 5.4 |
| $t$ | $[mm]$ | 0.125 |

Table 1: Material properties of Hexply IM7/8552

| Engineering constant | | Value |
|---|---|---|
| $E_1$ | $[GPa]$ | 1.3 |
| $\upsilon_{12}$ | – | 0.3 |
| $G_{12}$ | $[GPa]$ | 0.5 |

Table 2: Material properties of Scotch-Weld 9323 B/A

A quasi-isotropic stacking sequence was assigned identical to the test specimen. The composite laminate was connected to the adhesive using a tied interface. Furthermore, the Virtual Crack Closure Technique (VCCT) was used at the interface between the strap and the adhesive to extract the applied strain energy release rate in modes I, II and III. By adjusting the initially bonded nodes of the adhesive in the specimen longitudinal direction the change of $\Delta G$ and MMR can be tracked.

In order to reduce computational time a symmetric half model was used. Figure 1 summarizes the applied boundary conditions where, for better visualization, the shell elements are displayed with their physical thickness. The load was introduced by a line load having a magnitude corresponding to the maximum applied force during the fatigue test. Tabs used in the experiment were not modelled and the boundary constraints were applied at the end of the gauge length of the specimen.

Figure 2 presents the change of $\Delta G$ and MMR over specimen width, where it can be noted that the center of the specimen ($y = 0$) is loaded in mixed modes I and II with a MMR = 0.69. Closer to the edge of the specimen an additional mode III loading occurs, while mode I loading is being reduced. The total applied strain energy release rate $\Delta G_{tot}$ slightly increases towards the specimen edge. This behavior can be explained by the edge effect of the specimen, resulting in an additional bending moment around the specimen longitudinal direction.

For simplicity purposes only loading at the center line shall be considered for further examinations. Figure 2 shows the change in $\Delta G_{tot}$ and MMR with increasing crack length, while a crack length equal to 0mm shall correspond to the initial debond due to the Teflon foil.

It was found that loading of the adhesive is almost constant for a crack length of about 75mm. About 50mm in front of the clamping area $\Delta G_{tot}$ reduces while mode II loading becomes more dominant. Never-the-less a crack length of 90mm is considered to be within a representative measuring length.

It must be noted that the values of $\Delta G$ and MMR depend on the material properties of the adhesive and the modelling approach selected. For precise results further studies and material characterization tests are necessary. As the emphasis of this paper is on the experimental investigation, the presented values are considered to be sufficient.

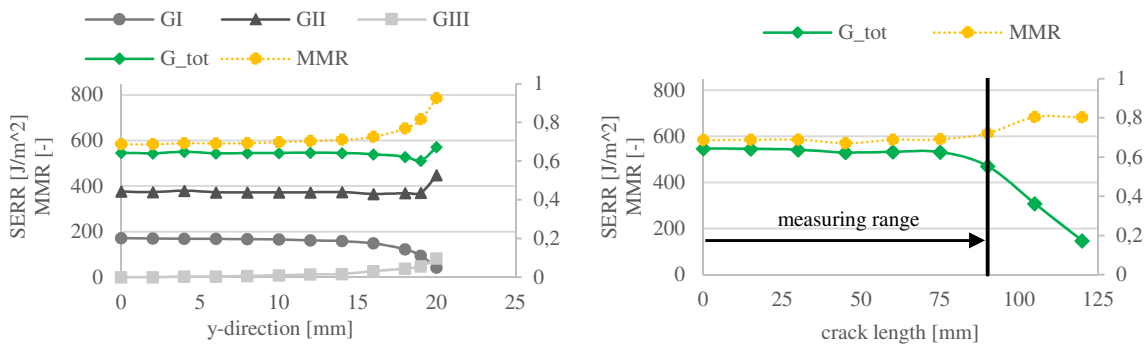


Figure 2: Plots of change ΔG and MMR with specimen width (left) and specimen length (right)

## 2.2 SPECIMEN MANUFACTURING

In a first step, the 16-ply laminate was manufactured. The fluoropolymer release film Airtech WL5200 [11] was applied on both sides of the laminate to ensure a reproducible surface quality as shown in Figure 4 . The stack was then cured in an autoclave using the autoclave cycle defined in the manufacturer's data sheet [12]. An additional pressure plate was used to create a plane surface on both sides of the laminate and to reduce its thickness variation.

Next the laminate was cut into three pieces as shown in Figure 3. These pieces were then cleaned with isopropanol and the surfaces treated using low pressure plasma. A preliminary study on surface treatment proved that due to application of a release foil, a significant amount of fluorine remains on the laminate surface, resulting in a rather low surface energy and prohibiting proper bonding of the adhesive to the adherends. By using low pressure plasma in the given configuration, adhesive failure can be avoided. Table 3 summarizes the parameters used for plasma treatment. [13]

After surface treatment the plates were adhesively bonded within 2 hours to fully exploit the benefits of surface activation. As shown in Figure 3 the base plate was therefore placed into a positioning device. By applying a thin Teflon coated tape at the designated location, an initial debond is ensured in the test specimen. Then, the adhesive is applied at the center of the base plate using a dog bone shape to ensure a proper distribution of the adhesive in the bondline and to avoid trapped air. The adhesive itself is applied using the manual application device Sulzer Mixpac DM 200-01 with the static mixing nozzle EPX-Mixing-Nozzle-200ml.

In order to control bondline thickness two precision thickness gage strips with a thickness of 0.5mm were placed along the outside length of the base laminate. Next, the lap laminate was applied and pre-compacted using an additional thick aluminum plate to ensure compressive loads were well distributed. For final compaction additional weights were used giving a pressure load of 1bar. The procedure was repeated for the doubler and the setup was then placed in an oven and cured for 2hrs at 65°C. For a balanced load distribution at the clamp, end tabs were bonded to the laminate using A10/B10 structural adhesive from the producer Lange & Ritter. Finally the test specimens were sawn using a precision diamond cutter.

## 2.3 DISCUSSION OF CRACK ARRESTING FEATURES

The capability of a rivetless nut plate joint as a CAF was investigated. For this the Cherry® Rivetless Nut Plate CNP53C3-1-03 designed for composite materials was used [14].

The rivetless nut plate joint is a mechanical fastener employed primarily in the aerospace industry. It requires a hole to be drilled in each adherend; one hole corresponds to the shaft diameter of the bolt and the other corresponds to the outer diameter of the nut plate sleeve. The retainer is then pressed into the associated adherend. A nut is placed into the retainer in a way that it can float and rotate to a certain extent, but is prevented from falling out. Finally, the adherends are joined together by a bolt. The corresponding bolt was selected according to the Military Standard MS983-11 and has a shaft diameter of 4.8mm. Figure 5 presents a micro-section of an adhesively bonded rivetless nut plate joint as well as a schematic illustration.

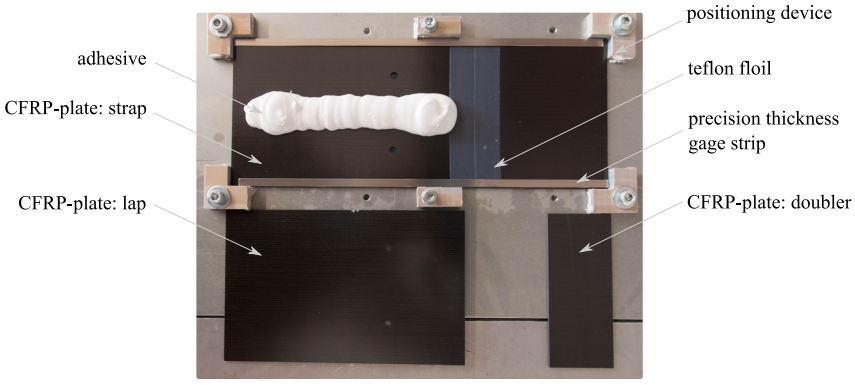


Figure 3: Manufacturing set-up for adhesive joining

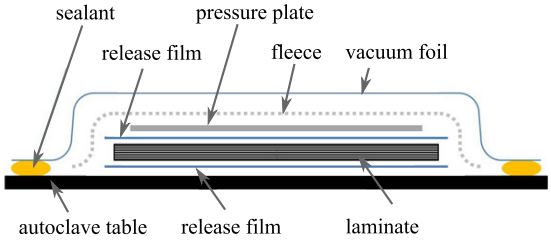


Figure 4: Schematic layout of laminate manufacturing

| Parameter | | Value |
|---|---|---|
| Working gas | – | $N_2$ |
| Duration of treatment | $[s]$ | 10 |
| Internal pressure | $[mbar]$ | 0.1 |
| Volumetric flow | $[sccm/min]$ | 50 |
| Power input | $[kW]$ | 1,0 |

Table 3: Parameters for low pressure plasma surface treatment

Due to expansion of the sleeve inside the hole, the rivetless nut plate meets NASM25027 torque-out and push-out requirements. Furthermore, it was shown that the fatigue life of the parent material can be enhanced. Finally, the assembly process is improved because access from only one side is needed, both adherends can be drilled separately and manufacturing tolerances are accounted for by the clearance between the bolt and the nut plate [14].

This combination of a rivetless nut plate joint with an adhesively bonded joint is not industrially used today. The manufacturing process was therefore defined for this study as follows and should be considered a laboratory process:

1. Drilling of holes and nut plate installation
2. Sealing of holes by applying tape on the outside of adherends. Perforation of tape to allow air to escape
3. Application of adhesive and pre-compaction until adhesive has spread over the entire bonding area
4. Insertion of bolts
5. Final compaction and tightening of bolt

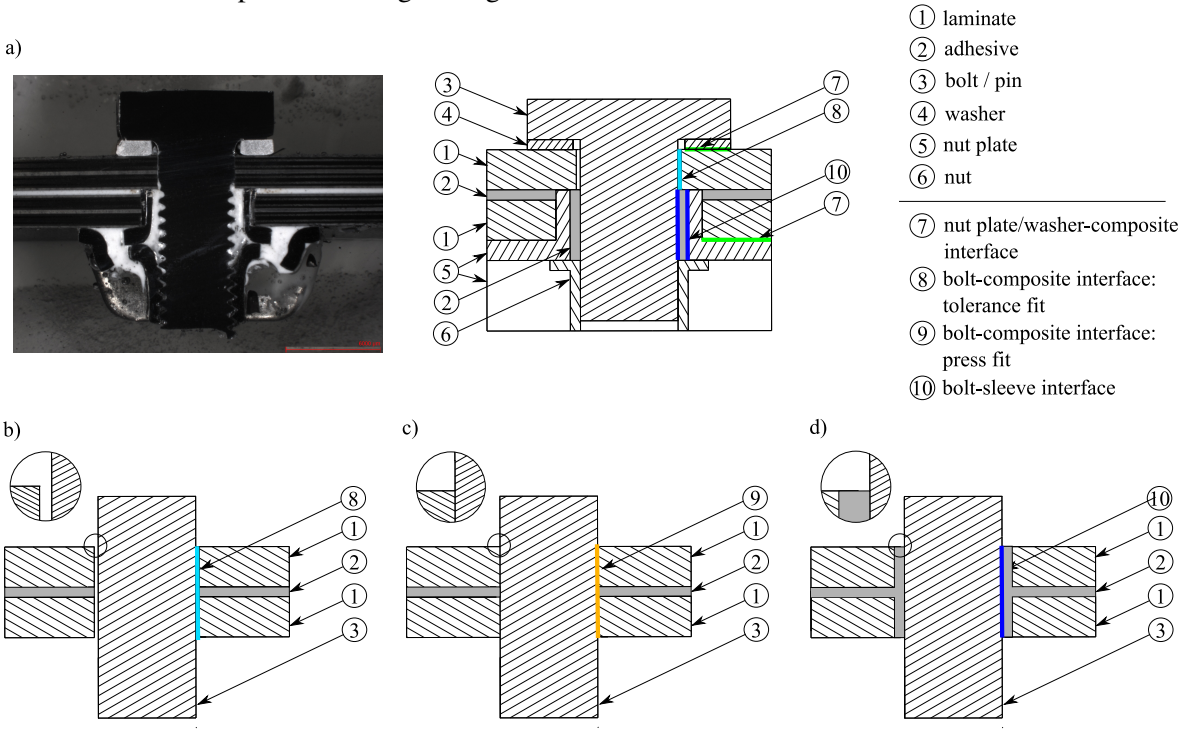


Figure 5: Crack Arresting Features a) rivetless nut plate joint b) pin with clearance fit c) pin with press fit d) adhesively bonded pin

For commonly used rivetless nut plates the sleeve length is selected to remain inside the adherend. Working with adhesive joints, however, requires a well-defined bondline thickness. For this reason the sleeve length was chosen to be 0.5mm longer than the adherend thickness, equal to the targeted bondline thickness, as shown in Figure 5. Using this approach the bolt can be tightened up to the point that the sleeve touches the opposing adherend.

From examining the rivetless nut plate joint in Figure 5, three principle load transfer mechanisms can be identified:

1. **Bolt-Composite Interface**:
   The hole corresponding to the adherend where no nut plate is installed is drilled using a diameter meeting approximately an h7/H7 clearance fit. Once this clearance is overcome during loading of the structure, due to the relative movement of both adherends, shear loads can be transferred. Due to the relatively high modulus of the adhesive, this load transfer can only be achieved once the crack arrives at, or has passed, the fastener.
2. **Bolt-Sleeve Interface**:
   A clearance of approximately 0.38mm is defined between the bolt and the sleeve of the nut plate. In order to achieve a shear transfer through the bolt and thereby a load reduction in the adhesive, bearing load transfer must be provided at the bolt-sleeve interface. The micro-section shown in Figure 5 proves that the manufacturing process was designed in a way so that adhesive flows into the space between bolt and sleeve. This can be considered a tight fit allowing bearing load transfer.
3. **Nut Plate/Washer-Composite Interface**:
   Due to the mechanics of the CLS specimen peeling forces open the joint. The nut-plate, as well as the washer, touch the composite restricting these opening modes. It is therefore expected that locally the mode I loading of the adhesive is significantly reduced. Additionally, shear loads can be transferred through the retainer and washer into the bolt.

The crack arresting mechanisms identified above can be summarized as follows:

- Local reinforcement through the mechanical joint and subsequent reduction of $\Delta G_{tot}$ acting at the adhesive
- Reduction of mode I loading in the adhesive

The effect of local reinforcement shall be investigated separately in detail. Different configurations of hybrid joints combining adhesive bonding and a pin as a mechanical fastener were therefore studied accounting for the different interfaces discussed for the adhesively bonded rivetless nut plate joint. Figure 5 presents a schematic illustration of the following configurations.

1. **Pin with Clearance Fit**:
   After adhesively bonding two plates, a hole is drilled using the same diameter and tolerance as for the Bolt-Composite Interface. A pin having the same diameter as the bolt shaft is then installed resulting in an h7/H7 clearance fit. In order to prevent the pin from falling out during fatigue testing, it is fixed using rubber O-rings on both sides. These rings were selected to ensure that no closing forces are acting which would be the case if metallic nuts were used.
2. **Pin with Press Fit**:
   The specimen is prepared equal to the configuration “pin with clearance fit” up to the point of installation of the pin. In this configuration, the actual diameter of the hole was measured by using a self-made gauge with a 0.01mm accuracy. The pins were then manufactured with a diameter 0.01mm wider than the hole diameter. Using liquid nitrogen the pins were cooled to shrink and inserted. Due to the subsequent thermal expansion, a press fit was achieved.
3. **Adhesively Bonded Pin**:
   With this configuration the bolt-sleeve interface is represented. Both plates were drilled using a diameter equal to the inner diameter of the rivetless nut plate sleeve. Before bonding, the holes were sealed by tapes from the outside and perforated to allow air to escape. After an initial pre-compaction the pins were installed. A positioning device was used to ensure a perpendicular and concentric alignment of the pin.

## 3 TEST SET UP

The fatigue tests were performed on a 25kN IST servo-hydraulic testing machine. Testing parameters for the force controlled constant amplitude fatigue test were selected as follows:

- $\boldsymbol{R-value} = 0.1$: to avoid compressive loads and possible buckling
- **Low frequency** $\boldsymbol{f} = 5Hz$
- $\boldsymbol{F_{max}} = 20kN$: corresponding to the targeted average strain level of $4000\mu strain$ in the unbonded laminate.

Fundamental to investigation of CAF's is measurement of the crack front and crack growth over the specimen width. To achieve this, two measurement systems shown in Figure 6 were used allowing in-situ measurements of the crack front.

**USB camera microscopes** were installed on both sides of the specimen. By painting the sides of the specimen in white and applying a scale to it, the opening crack is monitored. The measurement was done during testing close to the end of a defined number of cycles and afterwards by loading the specimen with a reduced static load. The advantage of measuring the crack position during testing is that a higher maximum load is acting leading to a wider opening of the crack. However, the picture rate was relatively low, thereby reducing the accuracy of the measurement. Measuring the crack at a lower static load allows pictures to be taken with subsequent post-processing for more details. This worked very well when no CAF was affecting the crack growth. However, due to the effect of some CAFs, mode I loading was reduced resulting in a reduced opening of the specimen. Additionally, only a reduced static load was applied to avoid creep of the adhesive. Consequently the actual crack front was much more difficult to determine.

An **automated air-coupled ultrasonic measurement system** was additionally installed into the test rig. The technique used was air-coupled ultrasound in slanted transmission mode (Figure 6). 207 kHz unfocussed probes (airstar®) were used to generate and receive the signal. The ultrasound generator and the stepper control unit are a custom-made system developed by the University of Kaunas. Due to the slanted setup of the transducers, guided waves were generated in the material. These waves are sensitive to any changes of the material properties such as stiffness and thickness. With this information the crack front propagating between the laminates can be monitored by x-y-scanning the specimen. In order to avoid ultrasound transmitting directly through air around the specimen, special shielding was installed during measurements. For this reason it is not possible to perform measurements during cyclic testing. The measurable area is slightly smaller than the width of the specimen due to edge effects and superposition of original and reflected wave. The lost area is 5 mm wide on each side of the specimen.

The result of an air-coupled ultrasound measurement is shown in Figure 6. Areas with higher amplitude are single and double layered sections of the specimen. Areas with low amplitude are delaminated sections. To determine the crack front, the signal sequence along the specimen length was evaluated. The crack length is determined as the distance between the mean values of the signal flanks.

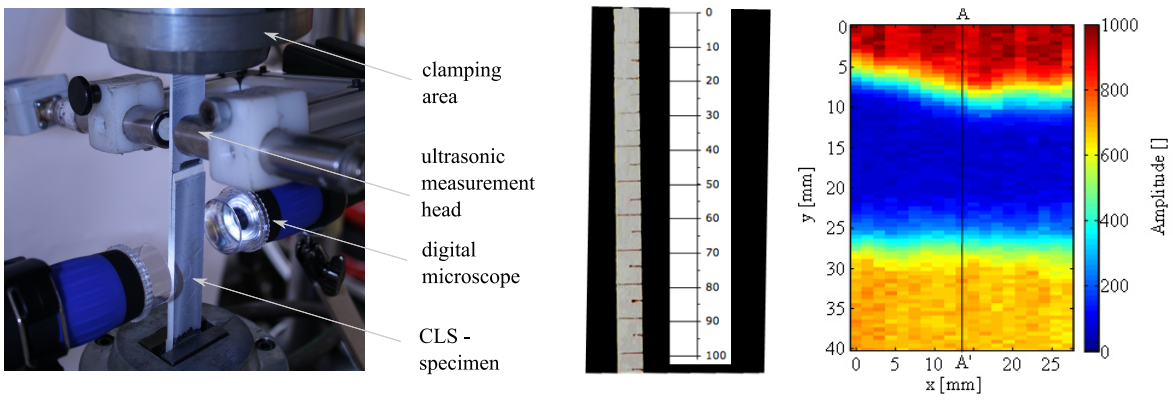


Figure 6: Test set up; example of measurement using digital microscope; example of ultrasound measurement [15] (left to right)

The actual test procedure was defined iteratively. A relative low number of cycles were used initially to determine the crack growth rate for the given specimen, from which subsequent measurement intervals were selected. Once the crack approaches the CAF the crack growth rate was in some cases significantly reduced, hence the measurement intervals were increased.

## 4 TEST RESULTS AND DISCUSSION

A screening test program was defined to provide a first inside into the crack arresting capabilities of the rivetless nut plate joint. The three hybrid joint configuration presented in Figure 5, combining adhesive bonding with a local reinforcement through a pin, were additionally tested to separately study the effect of local reinforcement within the rivetless nut plate joint.

In total two specimen were tested per configuration. The results are compared to purely adhesively bonded joints. Figure 7 presents the crack length with respect to the fatigue cycle. The crack length was measured using two USB camera microscopes on both edges of the specimen. The location of the CAF is included in the graphs to provide a reference for the changing crack growth behavior. In Figure 7, the following notations for the curves were used: **RN** – rivetless nut plate; **PC** – pin with clearance fit; **BP** – bonded pin; **PP** – pin with press fit; Bond – purely bonded.

Figure 8 presents the changing crack front shape over specimen width as determined with ultrasonic measurements. For better visualization the crack front is drawn on a photograph of the corresponding specimen.

During the test program it was observed, in many cases, that crack fronts did not propagate in parallel. For reasons of clarity, only the mean crack length between the optical measurements on the left and right hand side of the specimen are presented in Figure 7.

Finally, the crack growth behavior compared for all CAF configurations is also presented in Figure 7. Due to variations of the initial crack growth rate, a direct comparison is difficult. It was therefore decided to present the crack length with respect to the normalized fatigue cycle. The fatigue cycle is normalized by the fatigue cycles required to reach a crack length of 45mm, equal to the location of the CAF:

$$cycle_{norm} = \frac{cycle}{cycle_{@\ a=45mm}} \tag{4}$$

Based on the test results presented in Figure 7 and Figure 8 the following observations can be made:

1. An almost constant crack growth behavior was found in purely adhesively bonded CLS-specimen, supporting the initial assumption that was made based on numerical simulations.
2. For all four configuration of hybrid joints, the crack growth in front of the CAF was not influenced by the CAF.
3. Once the crack passes the CAF, it was slowed down. A transition zone can be identified which eventually leads to a crack growth rate slower than the initial one.
4. The magnitude of crack speed reduction strongly depends on the type of configuration:
   The **rivetless nut plate joint** virtually arrests the crack about 10mm behind the CAF.
   The **pin with press fit** also reduced the crack speed significantly. After the transition zone the crack propagates on the outside of the specimen about thirteen times slower than in front of the CAF.
   The **adhesively bonded pin** did not achieve a crack growth reduction as was achieved with the pin with press fit; however, it did reduce the crack growth rate by about a 50%.
   The **pin with clearance fit** showed similar crack arresting capability as the adhesively bonded pin. A transition zone similar to the other concepts was found and the crack growth was also reduced by about a factor of two.

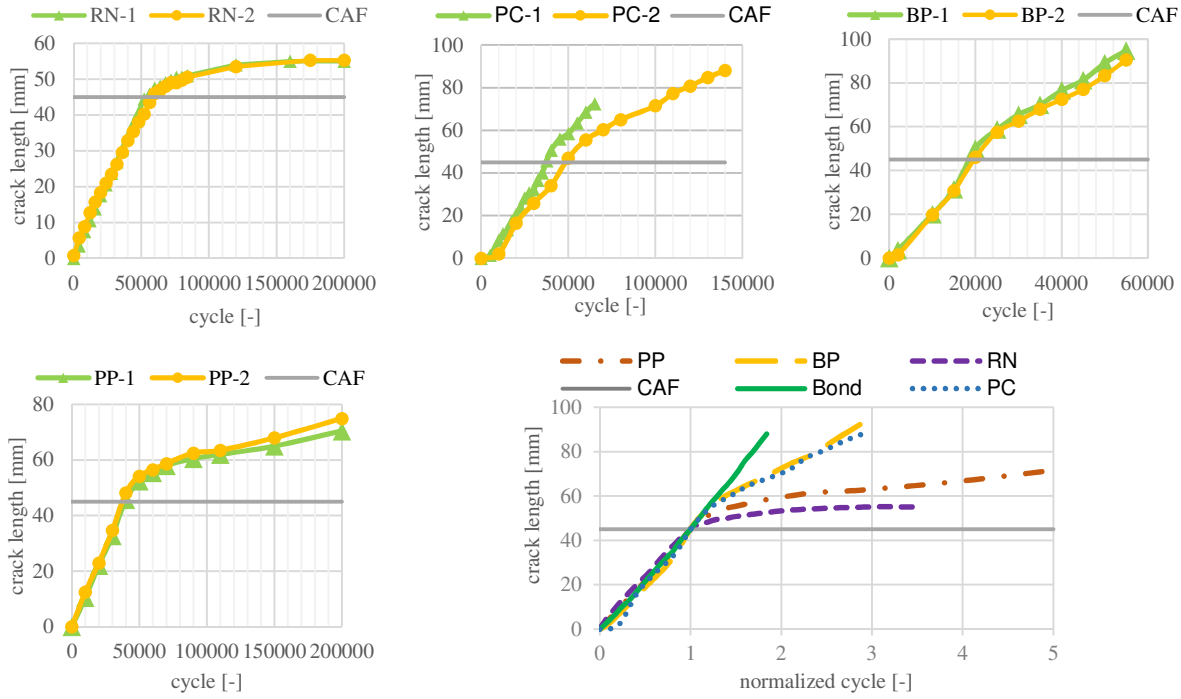


Figure 7: Change of crack length during fatigue test for hybrid joints using different CAF (top-left to bottom right): rivetless nut plate joint; pin with clearance fit; bonded pin; pin with press fit; comparison of hybrid joints with respect to $cycle_{norm}$

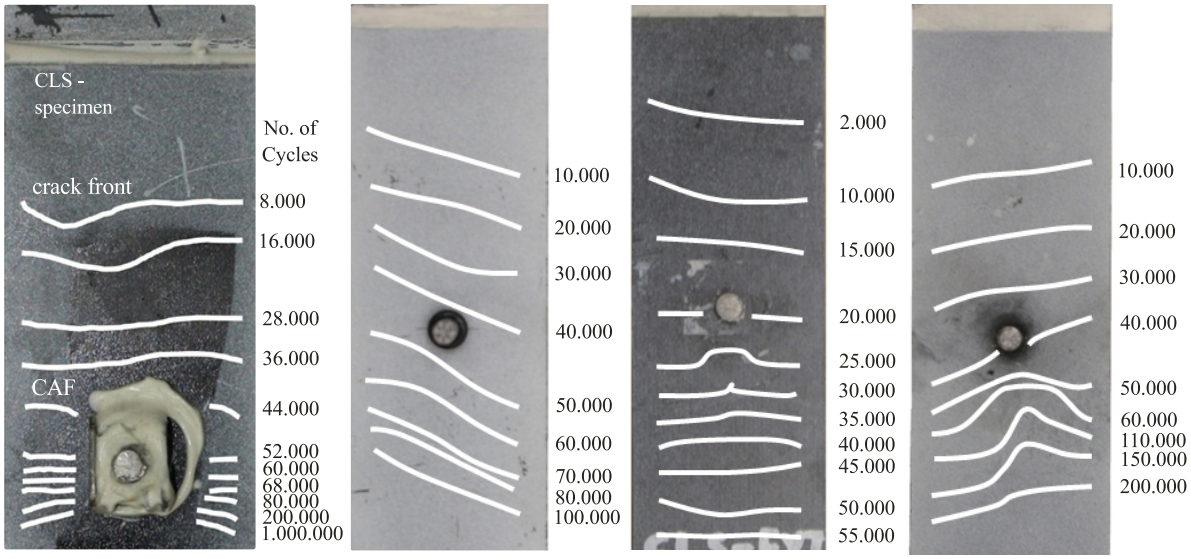


Figure 8: Crack front propagation of a hybrid joint configurations using different CAF (left to right): rivetless nut plate joint; pin with clearance fit; bonded pin; pin with press fit

5. The crack front shape various significantly for the different hybrid joint configurations.
   The **pins with press fit** resulted in a significant change of crack front shape. While the crack initially developed in a straight line, the crack speed was significantly reduced close to the center line of the specimen behind the CAF, leading to a curved crack front.
   A similar behavior was observed for the **adhesively bonded pins;** however, with an increasing crack front growth the crack front shape became straight again.
   The **pins with a clearance fit** did not affect the crack front shape.

Due to the large size of the retainer, the crack front close to the center line of the **rivetless nut plate joint** can unfortunately not be investigated using ultrasonic measurements.

During testing it was observed that the adhesively bonded pins detached on the inside of the hole; therefore opening of the specimen during loading was not efficiently suppressed. This is in contrast to what was observed for the pressed in pin. Here the friction forces between the pin and composite were so high, that locally the opening of the specimen was suppressed. On the other hand the pins installed with a clearance did also not efficiently suppress the opening mode.

Comparing the results of the rivetless nut plate joint to the different pin configurations, it is suggested that local reinforcement through the pin section can only partially contribute to the crack arresting capability. It is felt that the washer and the retainer have a significant contribution to crack stopping. They increase the load transfer into the bolt and therefore reduce loading of the adhesive and also effectively prevent the opening modes. Through investigation of the influence of pure mode 1 loading reduction these effects can be quantified in more detail.

## 5 CONCLUSIONS

The screening test results indicate excellent capabilities of the rivetless nut plate joint to arrest a fatigue crack within the adhesive bondline. While the crack was not influenced when approaching the CAF, it was slowed down when passing the CAF and was virtually stopped at around 10mm behind the rivetless nut plate joint.

Three hybrid joint configurations using a pin as CAF were additionally tested, focusing on three different configurations for the pin-to-composite interface. The influence of these CAF configurations on crack growth in the adhesive layer were found to differed strongly. In all cases, however, the crack was not influenced when approaching the pin. After a transition zone, the crack continued to propagate with a reduced speed. While the pressed in pin showed the most significant influence on crack growth, the pin installed with a clearance fit was least effective.

The results suggest that a tight fit between the pin and the adhesive is necessary for an efficient reduction of the crack speed. This improves the load transfer into the pin and also helps suppress the opening deformation modes.

## 6 ACKNOWLEDGEMENT

The support of the European Union Seventh Framework Programme (FP7/2007-2013), under grant agreement n° 314180 (Project BOPACS: Boltless Assembling of Primary Aerospace Composite Structures), is gratefully acknowledged.

## 7 REFERENCES


[1] Federal Aviation Administration, "AC 20-107B - Composite Aircraft Structures," 24 August 2010.

[2] Boltless assembling Of Primary Composite Structures (BOPACS), "Description of Work," EU FP7 Research Project, 2012.

[3] M. M. Abdel Wahab, "Fatigue in Adhesively Bonded Joints: A Review," *ISRN Materials Science,* vol. 2012, 2012.

[4] I. A. Ashcroft, J. P. Casa-Rodriguez and V. V. Silberschmidt, "A Model to Predict the Anomalous Fatigue Crack Growth Behaviour Seen in Mixed Mechanism Fracture," *The Journal of Adhesion,* vol. 86, pp. 522-538, 2010.

[5] M. Fernández, M. de Moura, L. da Silva and A. Marques, "Mixed-mode I + II fatigue/fracture characterization of composite bonded joints using the Single-Leg Bending test," *Composites: Part A,* vol. 44, pp. 63-69, 2013.

[6] S. Stelzer, R. Jones and A. Brunner, "INTERLAMINAR FATIGUE CRACK GROWTH IN CARBON FIBER REINFORCED COMPOSITES," in *19th INTERNATIONAL CONFERENCE ON COMPOSITE MATERIALS*, Montréal, 2013.

[7] S. Azari, M. Papini, J. Schroeder and J. Spelt, "The effect of mode ratio and bond interface on the fatigue behavior of a highly-toughened epoxy," *Engineering Fracture Mechanics,* vol. 77, pp. 395-414, 2010.

[8] M. Imanaka, K. Haraga and T. Nishikawa, "Fatigue Strength of Adhesive/Rivet Combined Lap Joints," *The Journal of Adhesion,* vol. 49, pp. 197-209, 1995.

[9] K. Y. Lin, L. Richard and W. Liu, "DELAMINATION ARREST FASTENERS IN AIRCRAFT COMPOSITE STRUCTURES," in *19th INTERNATIONAL CONFERENCE ON COMPOSITE MATERIALS* , Montréal, 2013.

[10] G. Kelly, "Quasi-static strength and fatigue life of hybrid (bonded/bolted) composite single-lap joints," *Composite Structures,* vol. 72, pp. 119-129, 2006.

[11] AIRTECH INTERNACTIONA INC., "WRIGHTLON 5200," technical data sheet, 2015.

[12] Hexcel, "HexPly 8552," technical data sheet, 2013.

[13] M. Miller, "Untersuchung des Einflusses verschiedener klimatischer Bedingungen und Oberflächenvorbehandlungen auf das Risswachstumsverhalten in CFK-Klebeverbindungen," Institut für Flugzeugbau, Stuttgart, 2015.

[14] Cherry Aerospace, 02 04 2015. [Online]. Available: http://www.cherryaerospace.com/.

[15] W. Adebahr, M. Rahammer, R. Sachse, S. Gröninger, M. Käß, M. Kreutzbruck and G. Busse, "Crack growth monitoring at CFK adhesive bondings," in *Proc. 24. Stuttgarter Kunststoffkolloquium*, 2015.

[16] A. Graner Solana, A. Crocombe and I. Ashcroft, "Fatigue life and backface strain predictions in adhesively bonded joints," *International Journal of Adhesion & Adhesives,* vol. 30, pp. 36-42, 2010.